MATERIALS SCIENCE

Sabatier principle in designing CO_2-philic but blocking membranes

Leiqing Hu[1,2,3], Asha Jyothi Gottipalli[1], Gengyi Zhang[1], Kieran Fung[4], Thien Tran[1], Narjes Esmaeili[1], Peihong Zhang[5], Yifu Ding[4], Kaihang Shi[1], Haiqing Lin[1]*

Gas transport through polymers follows the sorption-diffusion mechanism, and gas-philic functional groups are often incorporated into polymers to enhance its solubility selectivity and thus separation efficiency. In contrast, we report that polymers exhibiting strong chemisorption toward specific gas molecules can counterintuitively impede their diffusion, illustrated by experimental and simulation studies of CO_2 transport in cross-linked polyamines, paralleling the Sabatier principle observed in catalysis. The CO_2-philic polyamine membrane attains an unprecedented H_2/CO_2 selectivity of 1800, making it highly desirable for H_2 purification. The cross-linked polyamines exhibit excellent self-healing properties and processability for fabricating thin-film composite membranes, indicating great promise for industrial separations. Retarded transport by introducing strongly binding groups presents a promising route for designing membranes for various separations.

INTRODUCTION

Chemical separations account for up to 15% of the global energy consumption (*1*). Membrane technology has emerged as the frontier for industrial separations due to its inherently high energy efficiency and absence of chemical wastes (*2*–*4*). State-of-the-art commercial membranes are often based on polymers, where gas transport is governed by the sorption-diffusion model (*5*). Gas permeability of component A (P_A) is a combination of solubility (S_A) and diffusivity (D_A), and the selectivity of component A over B ($\alpha_{A/B}$) can be written as follows

$$\alpha_{A/B} = \frac{P_A}{P_B} = \left(\frac{S_A}{S_B}\right) \times \left(\frac{D_A}{D_B}\right) \quad (1)$$

Most polymers achieve high selectivity via strong size-sieving ability and high diffusivity selectivity, which inevitably decreases gas diffusivity and permeability (*5*–*7*). An effective strategy to overcome this selectivity/permeability trade-off is to introduce functional groups with affinity toward component A, improving S_A and S_A/S_B and thus $\alpha_{A/B}$. For example, H_2/CO_2 separation is a critical step in producing blue hydrogen from fossil fuels or green hydrogen from biomass on a large scale (*8*–*11*). Polymers containing CO_2-philic groups were developed to achieve high CO_2/H_2 solubility and thus permeability selectivity, such as poly(ethylene oxide) (PEO) (*12*) and polyamines (*4*, *13*). Similarly, palladium (Pd) nanoparticles (*14*) and nanorods (*15*) and single-atom metals (*16*) with strong H_2 affinity were incorporated in polymers to enhance H_2 solubility and thus H_2/CO_2 solubility selectivity to overcome the trade-off.

We report here a mechanism for achieving H_2/CO_2 separation properties above the upper bound by retarded transport of CO_2, as exemplified by cross-linked polyethylenimine (XLPEIs) prepared by branched polyethylenimine (PEI; 25 kg/mol) cross-linked in situ using hexamethylene diisocyanate (HMDI), as shown in Fig. 1. Polyamines have a strong affinity toward CO_2, and thus, they have been designed as sorbents for direct air capture of CO_2 (*17*–*20*) and even membranes to selectively remove CO_2 from mixtures with N_2 and H_2 saturated by water vapor (*4*, *21*). However, in this study, we observed that the interactions between CO_2 and amine groups are so strong that they form "ionic" cross-linking and impede CO_2 diffusion (Fig. 1A), leading to superior H_2/CO_2 selectivity. Similar phenomena have been observed in the optimization of catalysts described by the Sabatier principle, where too-strong or too-weak interactions between the catalysts and reactants reduce reactivity (*22*). Furthermore, the XLPEIs can be facilely fabricated into thin-film composite (TFC) membranes, which exhibit an unprecedented H_2/CO_2 selectivity of 1100, much higher than state-of-the-art polymeric and inorganic membranes. Our strategy of high affinity yet retarded transport unveils a route for designing high-performance membranes for various molecular separations.

RESULTS

Structure and pure-gas H_2/CO_2 separation properties of XLPEIs

Figure 1B shows the reaction between the —N═C═O groups in HMDI and the primary and secondary amines in PEI, converting the viscous liquid PEI to a transparent solid film (Fig. 1C). Figure 1D displays the Fourier transform infrared (FTIR) spectra of XLPEIs, and the appearance of two new peaks at 1530 and 1610 cm^{-1} (corresponding to the amide and carbonyl groups, respectively) and the disappearance of the characteristic peak of the isocyanate group at 2340 cm^{-1} confirm the reaction (*23*). In addition, the peak at 3300 cm^{-1} representing primary amine groups decreases from XLPEI10 to XLPEI20. The percentage of the reacted primary and secondary amines increases from 9.2% in XLPEI10 to 55% in XLPEI40 (table S1). Increasing the HMDI content increases the gel content (further validating the cross-linking), which reaches 90% at an HMDI content of 20% (Fig. 2A). Young's modulus also increases from 0.30 MPa in XLPEI10 to 10 MPa in XLPEI40 (fig. S1A and table S2).

Figure 2B shows that the cross-linking increases the density (ρ_P) of the dense XLPEI film determined using the buoyancy method and decreases the fractional free volume (FFV) calculated using

[1]Department of Chemical and Biological Engineering, University at Buffalo, The State University of New York, Buffalo, NY 14260, USA. [2]College of Environmental and Resource Sciences, Zhejiang University, Hangzhou 310058, China. [3]Zhejiang Provincial Key Laboratory of Air Pollution Monitoring and Synergestic Control, Hangzhou 310058, China. [4]Department of Mechanical Engineering, University of Colorado, Boulder, CO 80309, USA. [5]Department of Physics, University at Buffalo, The State University of New York, Buffalo, NY 14260, USA.
*Corresponding author. Email: haiqingl@buffalo.edu

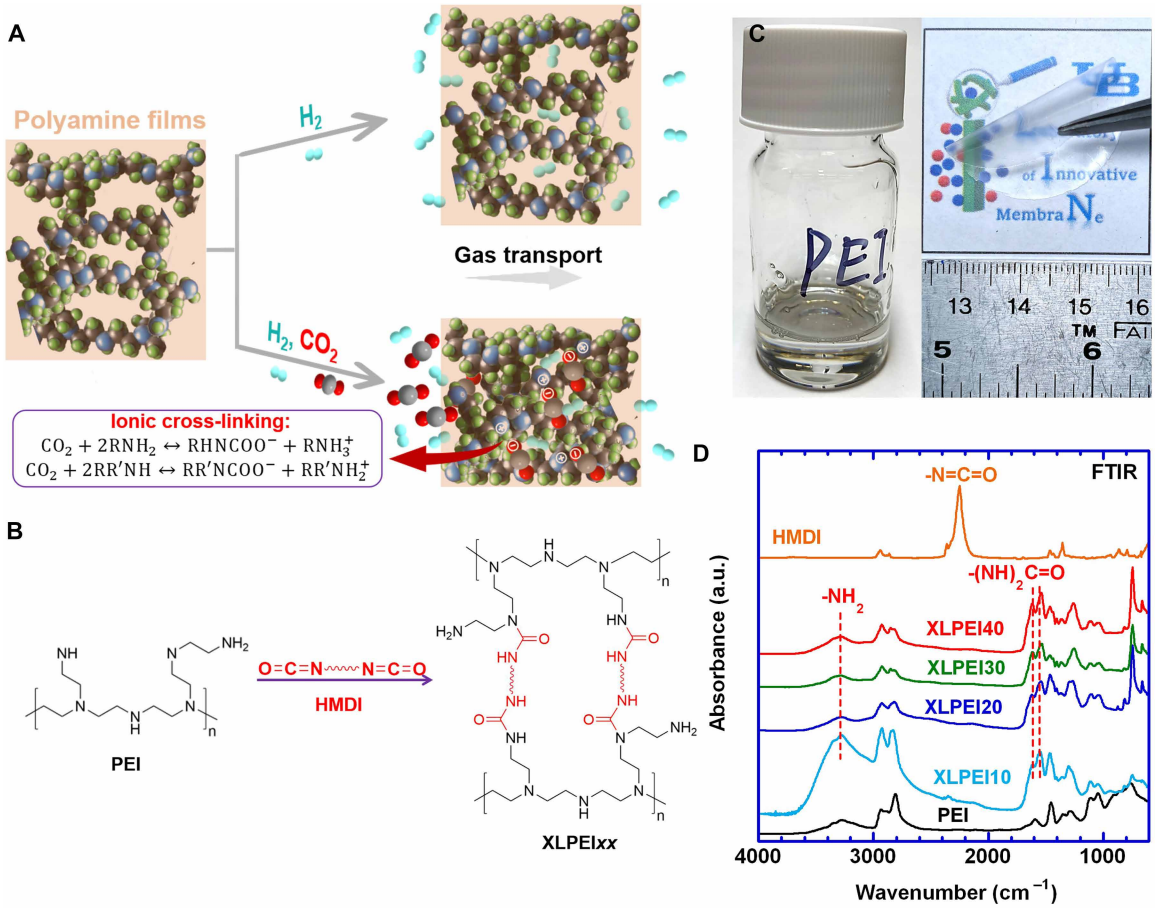

Fig. 1. CO_2-sticky XLPEIs with strong sorption but retarded diffusion. (**A**) Schematic illustration of H_2 and CO_2 permeation in polyamines. (**B**) Synthesis of XLPEIs from PEI and HMDI. (**C**) Photos of (left) PEI liquid and (right) an XLPEI30 film (50 μm thick). (**D**) FTIR spectra of XLPEIs. The samples are denoted as XLPEI*xx*, where *xx* is the mass percentage of HMDI in the samples. a.u., arbitrary unit.

FFV = 1 – 1.3$\rho_P V_w$, where V_w is the van der Waals volume estimated using the group contribution method (table S3). For instance, increasing the HMDI content from 0 to 40% increases the ρ_P from 1.030 to 1.210 g/cm^3 and decreases the FFV from 0.124 to 0.093. The decreased FFV is also consistent with the decreased *d*-spacing (or the average distance between polymer chains) from 4.5 to 4.3 Å (fig. S1B).

Increasing the HMDI content increases glass transition temperature (T_g) due to the increased cross-linking degree and decreased polymer chain flexibility (Fig. 2C), and all XLPEIs are rubbery at the temperatures of interest (35° to 150°C). Exposure to CO_2 at 8.0 atm and 100°C for 48 hours increases the T_g, confirming the reaction with CO_2 and the rigidified structures. In addition, as the HMDI content increases from 10 to 40 mass %, the degradation temperature with 5 mass % loss ($T_{d,5\%}$) increases from 179° to 212°C (fig. S1, C and D), indicating that the polymers can be used for H_2/CO_2 separation at temperatures up to 150°C. The increased degradation temperature with increasing HMDI content can be ascribed to the better thermal stability of C—C bonds than C—N bonds. For instance, polyethylene (PE) exhibits a $T_{d,5\%}$ of ~300°C, higher than that of PEI.

Figure 2 (D and E) depicts the strong CO_2 sorption at 100°C in the XLPEI films (~50 μm). Increasing the HMDI content decreases CO_2 solubility because of the reduced amine content in the XLPEIs, and their isotherms are shown in fig. S2A. Notably, CO_2 sorption in XLPEI20 and XLPEI30 does not reach equilibrium after 30 hours because of the extremely slow CO_2 diffusivity (*19*, *20*), so the final values at the 30th hour are used for convenience. Figure S2 (B and C) also exhibits that C_2H_6 solubility decreases with increasing HMDI content because of the decreased FFV. XLPEI20 demonstrates CO_2 solubility as high as 12 cm^3(STP) cm^{-3} atm^{-1} at 4.5 atm and 100°C, much higher than typical CO_2-philic polymers, such as cross-linked poly(ethylene glycol) diacrylate (XLPEGDA), poly(1,3-dioxolane) acrylate (PDXLA), and cellulose diacetate (CDA) (Fig. 2E and table S4). Similarly, XLPEIs show CO_2/C_2H_6 solubility selectivity as high as 7.0, despite their similar critical temperature, confirming the reaction between CO_2 and amine groups.

The CO_2 sorption behavior in XLPEI30 at different temperatures (60°, 90°, and 100°C) was investigated (fig. S2D). XLPEI30 appears to have higher CO_2 sorption at 100°C than at 60°C, which can be ascribed to the "ionic gelation" effect and its nonequilibrium nature (*19*, *20*). CO_2 molecules are first adsorbed onto the polymer surface and then react with the primary and secondary amines, forming COO^- and NH_3^+ ions and tightening the polymer structure (fig. S2E). This limits CO_2 diffusion into the bulk and hinders its approach to equilibrium, and the constraint becomes more pronounced at lower temperatures due to stronger CO_2 sorption on the surface and slower

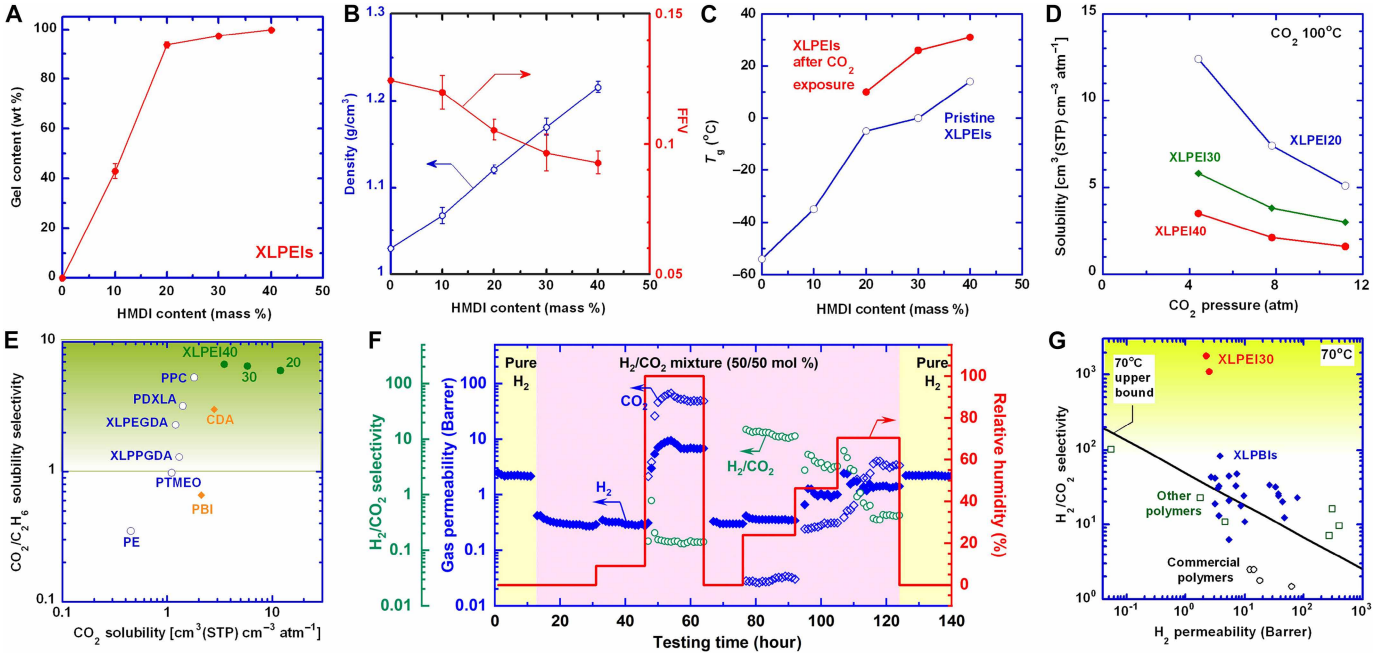

Fig. 2. Physical properties and pure-gas transport properties of XLPEI films. (**A**) Gel content. (**B**) Density and FFV. (**C**) Effect of the HMDI content and CO_2 exposure (at 8 atm and 100°C for 48 hours) on T_g. (**D**) CO_2 solubility as a function of pressure. (**E**) CO_2 solubility and CO_2/C_2H_6 solubility selectivity compared with other polymers, including glassy PBI (*32*) and CDA (*37*), and rubbery polymers such as PE (*38*), poly(tetramethylene oxide) (PTMEO) (*39*), cross-linked poly(propylene glycol) diacrylate (XLPPGDA) (*40*), XLPEGDA (*38*), PDXLA (*30*), and poly(propylene carbonate) (PPC) (*38*) (table S4). (**F**) H_2 and CO_2 permeability, and H_2/CO_2 selectivity of XLPEI30 films at 70°C and various relative humidity (RH) levels in 140 hours. CO_2 permeability is too low to be determined at RH levels below 9%. (**G**) H_2/CO_2 separation properties at 70°C compared with the upper bound and state-of-the-art polymers (table S7) (*6*, *16*).

CO_2 diffusivity. By contrast, increasing temperature enhances CO_2 diffusivity, allowing its access to the amine groups in the bulk and resulting in enhanced CO_2 sorption during the testing period (*24*). In addition, CO_2 permeability is too low to be determined in our apparatus at 100°C and below. Therefore, the highest values are used as estimates (table S5). In contrast, the polymers exhibit high H_2 permeability, which increases with rising temperature. However, introducing water vapor in the H_2/CO_2 mixture can exponentially increase CO_2 permeability in the XLPEI30 (Fig. 2F and table S6). In particular, with the saturated water vapor at 70°C, the XLPEI30 becomes CO_2-selective, exhibiting a CO_2 permeability of 48 Barrer [1 Barrer = 10^{-10} cm^3(STP)·cm cm^{-2} s^{-1} $cm\text{-}Hg^{-1}$] and CO_2/H_2 selectivity of 7.1. The behavior can be ascribed to the participation of water vapor in the reaction between CO_2 and amines, decreasing the reaction equilibrium constant and enhancing the reversibility of the reaction (or CO_2 desorption) (*25*). In addition, the film is swollen by the sorbed water, loosening chain packing (fig. S2F) and enhancing gas diffusion.

Figure 2G demonstrates superior H_2/CO_2 separation properties of XLPEI30, far surpassing Robeson's upper bound at 70°C (*26*, *27*). XLPEI30 exhibits H_2/CO_2 selectivity one order of magnitude higher than the leading polymers with strong size-sieving abilities, such as PBI and cross-linked PBI (table S7), showcasing the feasibility of using retarded CO_2 transport in designing highly selective membranes. Moreover, the H_2/CO_2 separation performance of XLPEI30 is comparable to leading inorganic materials, including nanoporous carbons, metal-organic frameworks, and two-dimensional materials (table S8 and fig. S3).

Noticeably, XLPEIs exhibit self-healing behavior because of their abundant hydrogen bonds (*28*, *29*), which can improve the manufacturability of defect-free TFC membranes. For instance, two XLPEI30 films were cut into two pieces and pinched with a needle to generate a pinhole of 0.7 mm in diameter (fig. S4). Compared with the pristine film with H_2 permeability of 0.39 Barrer at 35°C, both damaged samples exhibit similar H_2 permeability after self-healing (table S9), indicating complete healing from the damage.

Modeling and simulation of H_2 and CO_2 transport in XLPEIs

Figure 3A displays the effect of the temperature (35° to 100°C) on pure-gas H_2 permeability of XLPEIs, which is satisfactorily described using the Arrhenius equation (eq. S1). The activation energy value of H_2 permeation ($E_{P,A}$) increases from 29 kJ/mol for XLPEI20 to 44 kJ/mol for XLPEI40 (table S10), consistent with the decreasing FFV.

Although unexpected, the H_2/CO_2 separation properties in XLPEIs can also be described using a modified free-volume model. Within this framework, the FFV of the polymers during the exposure to CO_2 can be correlated with the T_g using the following equation (Fig. 3B) (*30*)

$$\mathrm{FFV} = \mathrm{FFV_g} + \alpha_r\left(T - T_g\right) \quad (2)$$

where FFV_g is the apparent FFV at T_g and is estimated at 0.089 for the XLPEIs. The α_r is the thermal expansion coefficient and is estimated at 4.9×10^{-4} K^{-1}, close to the estimated value (6.3×10^{-4} K^{-1}) from the aqueous PEI system (table S11 and eq. S2) (*31*). Increasing the HMDI content decreases pure-gas H_2 permeability at 35°C, which can be described using the free volume model (fig. S5)

$$P_A = A_p \exp\left(-B_p/\mathrm{FFV}\right) \quad (3)$$

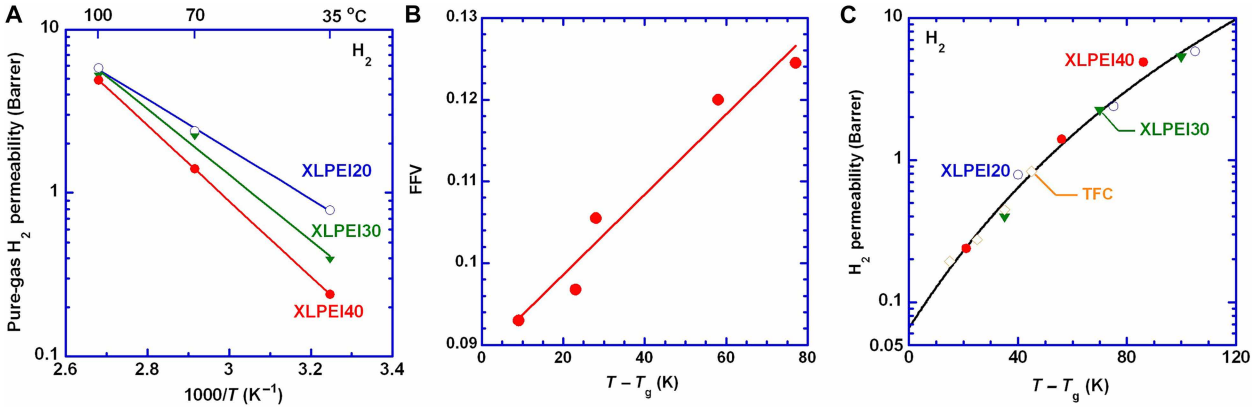

Fig. 3. Free volume model to describe H_2 permeability of XLPEI films. (**A**) Effect of temperature on H_2 permeability described using the Arrhenius equation. (**B**) Correlation of FFV with temperature and T_g. (**C**) H_2 permeability as a function of $(T - T_g)$ described using the VFT equation (Eq. 4). H_2 permeability of the TFC membranes was determined in a H_2/CO_2 mixture (50/50 vol %).

where A_P is a pre-exponential factor, and B_P is a constant depending on the penetrant size. Combining Eqs. 2 and 3 renders the following expression like the Vogel-Fulcher-Tammann (VFT) equation used to describe ion transport in rubbery polymers (*30*)

$$P_A = A_P \exp\left[\frac{-B_P/\alpha_r}{FFV_g/\alpha_r + (T - T_g)}\right] \quad (4)$$

Figure 3C shows that the H_2 permeability of XLPEIs at different temperatures (35° to 100°C) can be satisfactorily modeled using the VFT equation with an A_P value of 18,000 Barrer and B_P value of 1.1, indicating that H_2 transport in XLPEIs depends on the polymer chain mobility.

To understand the effect of strong CO_2 sorption on its transport and H_2/CO_2 selectivity in XLPEIs, H_2 and CO_2 sorption on monomer structures of specific rubbery polymers are simulated and compared (Fig. 4A and fig. S6). The primary amines on the branched PEI exhibit a CO_2 binding energy of −53 kJ/mol, much lower than that for other chemicals, such as nonane (−11 kJ/mol) and ethylene glycol (−16 kJ/mol) (table S12). On the other hand, H_2 binding energy on branched PEI is estimated at −5.0 kJ/mol, close to those for other chemicals but much lower than CO_2 binding energies. Consequently, the polymers exhibit a volcano trend of CO_2 permeability (Fig. 4B) and an inverted volcano trend of H_2/CO_2 selectivity (fig. S7) as a function of the binding energy with a facilitated transport zone and a retarded transport zone. Notably, the retarded transport can also be partially attributed to the tightened chain packing (or increased T_g) of the polymers (Fig. 2C).

To understand the retarded transport at molecular level, H_2 and CO_2 transport through a nanoporous graphene membrane was simulated using molecular dynamics (MD) simulations (Fig. 4C; figs. S8 to S11; tables S13 to S19; and movies S1 to S3), with adjustable adsorption energies toward CO_2 [$E_{ads}(CO_2)$] from −9.3 to −190 kJ/mol and pore diameters from 4.3 to 9.3 Å. Generally, CO_2 permeability increases with $E_{ads}(CO_2)$ decreasing from −9.3 to −37 kJ/mol because the enhanced affinity toward CO_2 can facilitate CO_2 transport in the membrane (Fig. 4, D to F). However, a further decrease of $E_{ads}(CO_2)$ generates irreversible bonding of CO_2 molecules on the graphene, thus impeding CO_2 diffusion (Fig. 4G). As such, CO_2 permeability decreases considerably, especially for the membrane with smaller pores, leading to a volcano trend with a threshold value of $E_{ads}(CO_2)$ at about −37 kJ/mol. On the other hand, H_2 permeability dramatically decreases along with the decreasing $E_{ads}(CO_2)$ due to the competitive sorption and pore blocking by adsorbed CO_2 (fig. S12A). As such, H_2/CO_2 selectivity decreases with $E_{ads}(CO_2)$ as well (fig. S12B).

Superior H_2/CO_2 separation performance of XLPEI TFC membranes

As XLPEI30 exhibits a balanced H_2 permeability and H_2/CO_2 selectivity, it was fabricated into TFC membranes via a scalable dip-coating method (*14*). The XLPEI30 layer has an average thickness of 450 nm on a modified polydimethylsiloxane (mPDMS) gutter layer supported by polyacrylonitrile porous support (Fig. 5A). Gas permeance of the membrane decreases with increasing penetrant size except for CO_2 (Fig. 5B). Specifically, CO_2 with a kinetic diameter of 3.3 Å exhibits lower gas permeance than O_2 (3.46 Å), further confirming the retarded CO_2 transport. The membrane shows H_2 permeance of 5.5 GPU (gas permeation unit) [1 GPU = 10^{-6} cm^3(STP) cm^{-2} s^{-1} cm-Hg^{-1}] and CO_2 permeance of 0.0052 GPU, leading to H_2/CO_2 selectivity of 1100, the highest reported for known polymers. In addition, based on its thickness, the XLPEI30 layer is estimated to have H_2 and CO_2 permeability of 2.5 and 0.0023 Barrer, respectively, consistent with the values obtained for the freestanding films. The membrane exhibits a pure-gas H_2/N_2 selectivity of 1800, much higher than state-of-the-art polymers (fig. S13 and table S20), indicating the strong molecular sieving capability of XLPEI30.

The membrane was further evaluated with various H_2/CO_2 mixtures at 9.0 atm and 70°C. Figure 5C shows that the mixed-gas H_2 permeance slightly decreases from 0.78 to 0.60 GPU with increasing CO_2 partial pressure from 2.2 to 7.3 atm. The mixed-gas H_2 permeance is much lower than the pure-gas value (where CO_2 partial pressure is 0 atm) because of the ion cross-linking of the XLPEI30 by the sorbed CO_2 during the mixed-gas permeation. Higher CO_2 partial pressure increases the CO_2 sorption and cross-linking degree and decreases the free volume, decreasing gas permeance but retaining mixed-gas H_2/CO_2 selectivity at 100 (Fig. 5D).

Industrial syngas streams are often at high temperatures, and thus, H_2/CO_2 separation is preferred at high temperatures to avoid cooling, which increases the costs (*32*). To this end, our TFC membranes were investigated at 60° to 90°C due to their optimal separation properties. Both H_2 and CO_2 permeances can be reversibly changed in this temperature range (fig. S14A). Figure 5E shows

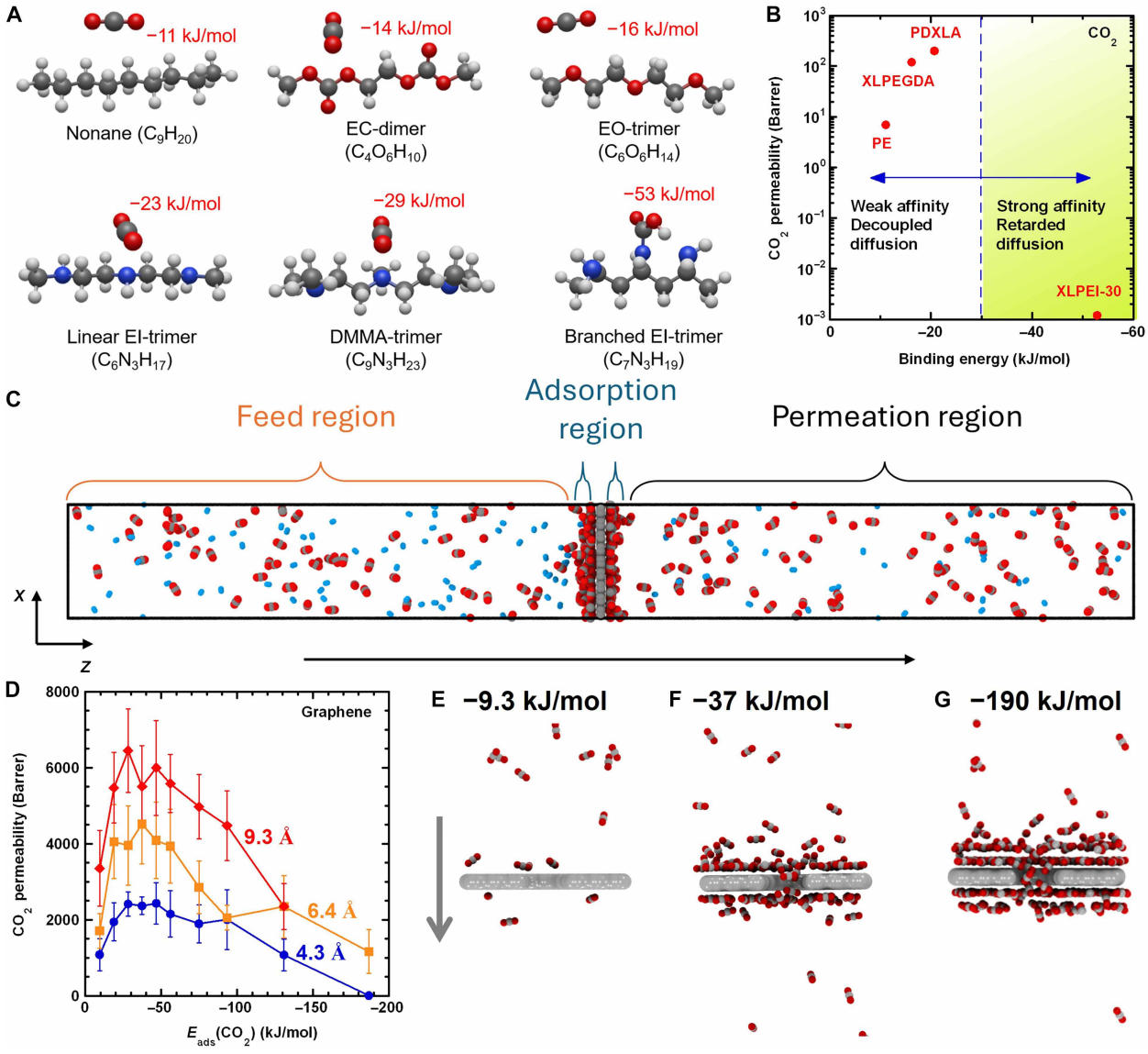

Fig. 4. Simulation of H_2 and CO_2 transport in model chemicals and porous graphene. Density functional theory (DFT) simulations of interactions between gas and XLPEIs, including (**A**) schematics and (**B**) CO_2 permeability as a function of CO_2 binding energy in polymers. Here, nonane, ethylene carbonate (EC)–dimer, ethylene oxide (EO)–trimer, linear ethylenimine (EI)–trimer, *N*,*N*-dimethyl-methylamine (DMMA)–trimer, and branched EI-trimer represent PE, poly(ethylene carbonate) (PEC), PEO, linear PEI, poly(*N*,*N*-dimethyl-methylamine) (PDMMA), and branched PEI, respectively. MD simulations of equimolar H_2/CO_2 mixture permeating through a nanoporous graphene membrane, including (**C**) a representative simulation snapshot where red beads represent oxygen atom, gray beads represent carbon atom, and blue beads represent hydrogen atom (M bead in the hydrogen model is not shown for clarity); (**D**) mixed-gas CO_2 permeability as a function of CO_2 adsorption energy [$E_{ads}(CO_2)$] in simulated nanoporous graphene membranes with pore diameter from 4.3 to 9.3 Å (error bars were calculated from 10 replicate runs); and simulation snapshots of CO_2 transport in membranes with a pore diameter at 6.4 Å and various $E_{ads}(CO_2)$ values, including (**E**) −9.3 kJ/mol, (**F**) −37 kJ/mol, and (**G**) −190 kJ/mol.

that mixed-gas H_2 and CO_2 permeance increases with increasing temperature due to the increased gas diffusivity, and the increase can be satisfactorily described using the Arrhenius equation. Mixed-gas selectivity increases with decreasing temperature, reaching 190 at 60°C, resulting in a lower $E_{P,A}$ value for H_2 (48 kJ/mol) than CO_2 (95 kJ/mol) because of the smaller kinetic diameter for H_2. The $E_{P,A}$ value for the mixed-gas H_2 permeation is also higher than that of pure-gas permeation (38 kJ/mol) because of the increased chain rigidity by CO_2 cross-linking. Furthermore, the mixed-gas H_2 permeance can be used to estimate T_g (45°C) using the VFT equation (table S21), higher than the experimentally measured T_g of 26°C (Fig. 2C). This difference is likely attributed to the potential partial release of CO_2 from the XLPEI30 film before the differential scanning calorimetry (DSC) analysis. Using the estimated T_g values, we can effectively model mixed-gas permeance and H_2/CO_2 selectivity using the VFT equation (Fig. 3C and fig. S14, B and C). Notably, the B_P value is 2.1 for CO_2 permeability, higher than that (1.1) for H_2 permeability because of the larger kinetic diameter for CO_2.

The long-term stability of the TFC membrane was investigated using both pure and mixed gases (Fig. 5F). The membrane exhibits stable mixed-gas separation performances for 15 hours before switching to pure H_2. Pure-gas H_2 permeability gradually recovers

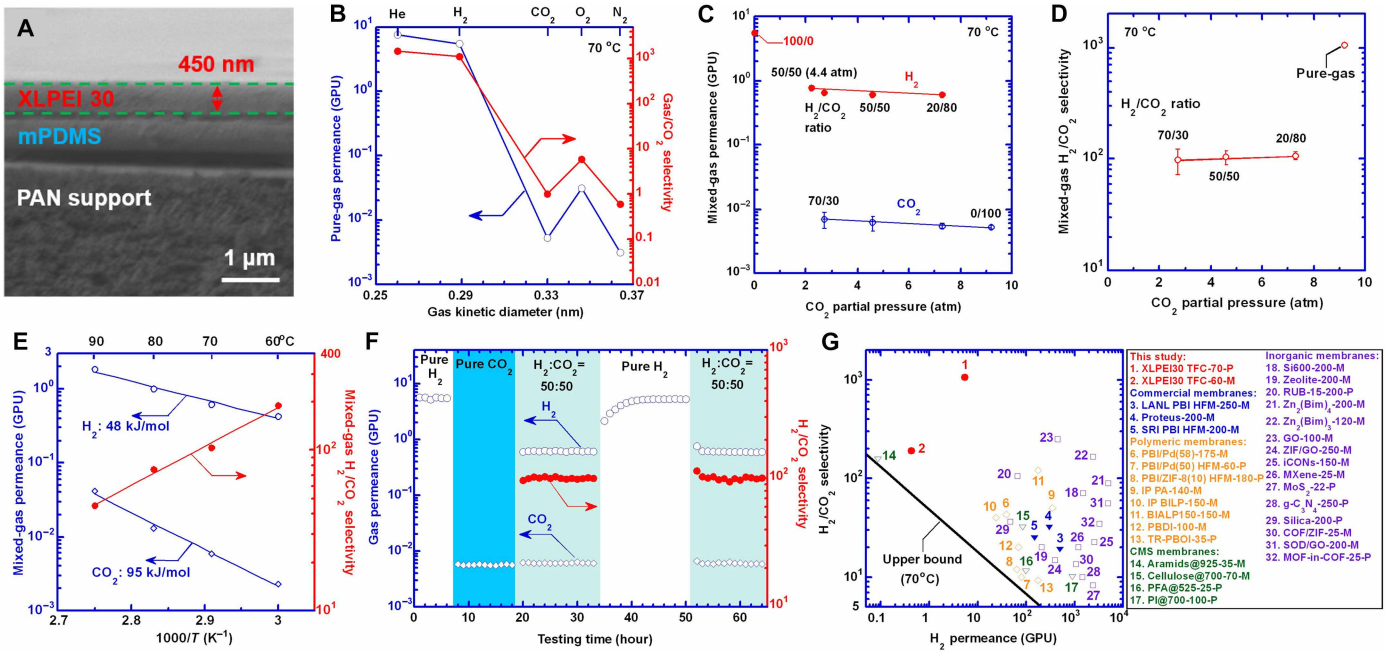

Fig. 5. Superior H_2/CO_2 separation performance of XLPEI30 TFC membranes. (**A**) Cross-sectional scanning electron microscopy image. (**B**) Gas permeance as a function of kinetic diameter at 70°C and 9 atm. (**C**) Mixed-gas permeance and (**D**) H_2/CO_2 selectivity as a function of the feed CO_2 partial pressure at 70°C and 9 atm. (**E**) Effect of temperature on H_2/CO_2 separation properties with H_2/CO_2 of 50:50 at 9 atm. (**F**) Long-term stability under pure-mixed-pure-gas conditions in the presence of water vapor at 9 atm and 70°C for 65 hours. (**G**) Comparison with the state-of-the-art membranes (table S22), including leading membranes (LANL PBI HFM, Proteus-200, and SRI PBI HFM), polymeric membranes [PBI/Pd(58) (*14*), PBI/Pd(50) HFM (*41*), PBI/ZIF-8(10) HFM (*42*), IP PA (*43*), IP BILP (*44*), BIALP150 (*11*), PBDI (*45*), and TR-PBOI (*46*)], carbon molecular sieve (CMS) membranes [Aramides@925 (*47*), cellulose@700 (*48*), PFA@525 (*49*), and PI@700 (*50*)], and inorganic membranes (table S8). The values after the dash represent the testing temperature (°C). The upper bound at 70°C was drawn assuming 1-μm-thick selective layers.

within 6 hours, validating the reversible CO_2 cross-linking. In the second-cycle mixed-gas separation after 50 hours, the membrane exhibits similar separation performance, indicating that it is stable against physical aging or CO_2 plasticization. Notably, it is rather fast for H_2 permeance to reach stable values when switching from pure H_2 to the H_2/CO_2 mixture, as CO_2 sorption on the surface can immediately reduce H_2 permeance; by contrast, it takes much longer time for H_2 permeance to recover after the switch from the mixture to pure H_2 due to the slow kinetics for the sorbed CO_2 in the bulk to desorb and diffuse to the surface. Similarly, as the temperature decreases from 90° to 60°C, the mixed-gas permeance takes several hours to stabilize due to the decreased CO_2 diffusivity and desorption kinetics (fig. S14A).

Figure 5G compares the H_2/CO_2 separation performance of the XLPEI30 membrane with state-of-the-art TFC membranes [including commercial membranes, polymeric membranes, polymer-derived carbon molecular sieve (CMS) membranes, and inorganic membranes], benchmarking with the upper bound at 70°C (*6*, *32*). Most membranes exhibit high H_2 permeances at higher temperatures. Nevertheless, our XLPEI30 membrane exhibits the highest H_2/CO_2 selectivity for mixed-gas separations, far surpassing the upper bound and all polymer-based TFC membranes. The separation property of XLPEI30 is also comparable to many leading inorganic membranes.

DISCUSSION

We report that strong gas chemisorption can reversely retard its transport, uncovering a way to design highly selective materials for molecular separations. This phenomenon is illustrated by CO_2 transport in XLPEI membranes, which contain numerous amine groups that have a strong interaction with CO_2, as evidenced by a binding energy of −53 kJ/mol. The ionic cross-linking formed by CO_2 chemisorption in XLPEI increases polymer chain rigidity and decreases CO_2 permeability, leading to H_2/CO_2 selectivity up to 1800, the highest value reported so far. Moreover, the XLPEIs can be facilely fabricated into scalable TFC membranes, and they show stable separation properties when challenged with simulated syngas. This work raises the prospect of designing reactive materials with retarded diffusion for other important gas separations.

MATERIALS AND METHODS

Materials

Branched PEI (molecular weight: ~25,000 g/mol), HMDI, dopamine hydrochloride, hexane, isopropyl alcohol, iso-octane, and chloroform were purchased from Sigma-Aldrich Corporation (St. Louis, MO). Tris(tromethamine) was purchased from Thermo Fisher Scientific (Pittsburgh, PA). Sylgard 184 was procured from Dow Silicones (Midland, MI). Polysulfone (PSF) porous support with a molecular weight cutoff of 20 kDa was purchased from Sterlitech (Auburn, WA). Gas cylinders of H_2, CO_2, and N_2 with ultrahigh purity were acquired from Airgas Inc. (Buffalo, NY).

Preparation of freestanding films and TFC membranes of XLPEIs

Freestanding films of XLPEIs were prepared via a solution synthesis and casting method. First, 2 mass % PEI/chloroform and 1 mass % HMDI/chloroform solutions were prepared separately. Second, the

HMDI solution was added dropwise to the PEI solution under sonication. The mass ratio of HMDI to PEI was varied at 20:80, 30:70, and 40:60. Third, the mixed solution was cast in a Teflon petri dish and dried at 60°C under N_2 atmosphere. Last, a freestanding film with an average thickness of 50 μm was obtained.

To prepare TFC membranes, an XLPEI30 solution containing 1.1 mass % PEI and 0.46 mass % HMDI in chloroform was first prepared. Second, the PSF support was coated with a gutter layer of PDMS followed by the modification by dopamine using a procedure reported in our prior study (*33*). Last, the membrane was dip-coated twice with the XLPEI30 solution for 1 s and dried under N_2 at 23°C for 4 hours before tests.

Characterizations of XLPEIs

FTIR spectra were collected between 600 and 2500 cm^{-1} using a Vertex 70 Burker spectrometer (Bruker Scientific LLC, Billerica, MA). Thermal transitions (including T_g) were measured using DSC (Q2000, TA Instruments, New Castle, DE) and Universal Analysis 2000 software. The wide-angle x-ray diffraction patterns were obtained using an Ultima IV x-ray diffractometer (Rigaku Corporation, Tokyo, Japan) and CuKα radiation with a wavelength of 1.54 Å. A TG 209 F1 Iris Netzch thermogravimetric analysis was used to determine thermal stability at temperatures up to 600°C under an N_2 flow. The gel content of the XLPEI films was the fraction of the residual sample after immersing in chloroform at 35°C for 24 hours. The density of XLPEI films was determined using Archimedes' principle with iso-octane as an auxiliary liquid. Mechanical properties of XLPEI films were determined using static tensile loading at ≈22°C by a universal testing system (Instron 5965, Instron Mechanical Testing Systems, USA). Three specimens (15 mm by 5 mm) were tested with a uniaxial tensile load and an initial strain of 0.1% at 1.0% min^{-1} until they fractured. Young's modulus is calculated from the slope in the elastic deformation region of the stress-strain curve, where the tensile strength and fracture strain can also be estimated.

The self-healing properties of XLPEI30 films were demonstrated via two approaches. In the first approach, an XLPEI film (sample 1) of ~1 by 2 cm was cut into two pieces using a surgical knife. The cut interfaces were brought into contact with each other and then exposed to moisture at 22°C for 6 hours. In the second approach, another XLPEI30 film was first tested for gas permeation. Afterward, a hole of a 0.7 mm was punctured in the middle of the film using a needle. Following this, the sample was exposed to moisture at 22°C for 6 hours and dried overnight. Last, the sample was retested for gas permeation.

For freestanding XLPEI films, pure-gas permeability was determined using a constant-volume and variable-pressure permeation apparatus at 35° to 100°C, and pure-gas sorption isotherms were determined using a gravimetric sorption analyzer of IGA 001 (Hiden Isochema, UK) (*27*). Gas diffusivity was calculated based on the solution-diffusion model and summarized in table S12. For TFC membranes, pure- and mixed-gas permeability was measured using a constant-pressure and variable-volume permeation apparatus at various temperatures with N_2 as the sweep gas on the permeate side at ~1 atm. The gas composition on the sweep side was determined using a gas chromatograph. Mixed-gas permeability of XLPEI30 films was measured using the same approach at 70°C.

Binding energy calculation and MD simulation

Density functional theory (DFT) calculations of the sorption energies are carried out using the Quantum ESPRESSO package (*34*, *35*). The van der Waals (vdw) interaction is included in the calculations within the vdw–density functional (vdw-DF) method using the vdW-optB86b functional (*36*). The sorption energies of H_2 and CO_2 are studied on six model molecules that capture the important chemistry and structural features of the membrane. Those molecule structures are nonane, ethylene carbonate (EC)–dimer, ethylene oxide (EO)–trimer, linear ethylenimine (EI)–trimer, *N*,*N*-dimethyl-methylamine (DMMA)–trimer, and branched EI-trimer, respectively representing PE, poly(ethylene carbonate) (PEC), PEO, linear PEI, poly(*N*,*N*-dimethyl-methylamine) (PDMMA), and branched PEI. For each model molecule, the CO_2 and H_2 are placed at various sorption sites, and the structures are fully optimized until the residual forces acting on all atoms in the system are smaller than 10^{-3} eV/Å. The details of the MD simulation on gas transport via graphene membranes were listed in the Supplementary Materials.

Supplementary Materials

The PDF file includes:

Supplementary Text
Figs. S1 to S14
Tables S1 to S22
Legends for movies S1 to S3
Legend for code S1
References

Other Supplementary Material for this manuscript includes the following:

Movies S1 to S3
Code S1

REFERENCES AND NOTES

1. D. S. Sholl, R. P. Lively, Seven chemical separations to change the world. *Nature* **532**, 435–437 (2016).
2. G. Chen, C. Chen, Y. Guo, Z. Chu, Y. Pan, G. Liu, G. Liu, Y. Han, W. Jin, N. Xu, Solid-solvent processing of ultrathin, highly loaded mixed-matrix membrane for gas separation. *Science* **381**, 1350–1356 (2023).
3. H. W. Lai, F. M. Benedetti, J. M. Ahn, A. M. Robinson, Y. Wang, I. Pinnau, Z. P. Smith, Y. Xia, Hydrocarbon ladder polymers with ultrahigh permselectivity for membrane gas separations. *Science* **375**, 1390–1392 (2022).
4. M. Sandru, E. M. Sandru, W. F. Ingram, J. Deng, P. M. Stenstad, L. Deng, R. J. Spontak, An integrated materials approach to ultrapermeable and ultraselective CO_2 polymer membranes. *Science* **376**, 90–94 (2022).
5. H. Park, J. Kamcev, L. M. Robeson, M. Elimelech, B. D. Freeman, Maximizing the right stuff: The trade-off between membrane permeability and selectivity. *Science* **356**, eaab0530 (2017).
6. L. Hu, W. I. Lee, K. Chen, S. Roy, K. Fung, K. Kisslinger, E. Deng, Y. Ding, P. M. Ajayan, C. Y. Nam, H. Lin, Atomically fine-tuning organic-inorganic carbon molecular sieve membranes for hydrogen production. *ACS Nano* **19**, 4663–4671 (2025).
7. K. Hazazi, Y. Wang, B. Ghanem, X. Hu, T. Puspasari, C. Chen, Y. Han, I. Pinnau, Precise molecular sieving of ethylene from ethane using triptycene-derived submicroporous carbon membranes. *Nat. Mater.* **22**, 1218–1226 (2023).
8. X. Li, C. Jiao, X. Zhang, X. Xu, S. Gul, F. Liang, J. Caro, H. Jiang, Zinc coordination-polymer-mediated self-assembly of nanoparticles into "Brick-and-Mortar" membranes for hydrogen separation. *Angew. Chem. Int. Ed. Engl.* **64**, e202416919 (2025).
9. S. Song, Q. Liu, S. Swathilakshmi, H. Y. Chi, Z. Zhou, R. Goswami, D. Chernyshov, K. V. Agrawal, High-performance H_2/CO_2 separation from 4-nm-thick oriented Zn_2(benzimidazole)$_4$ films. *Sci. Adv.* **10**, eads6315 (2024).
10. Z.-A. Qiao, S.-H. Chai, K. Nelson, Z. Bi, J. Chen, S. M. Mahurin, X. Zhu, S. Dai, Polymeric molecular sieve membranes via in situ cross-linking of non-porous polymer membrane templates. *Nat. Commun.* **5**, 3705 (2014).
11. X. Yan, T. Song, M. Li, Z. Wang, X. Liu, Sub-micro porous thin polymer membranes for discriminating H_2 and CO_2. *Nat. Commun.* **15**, 628 (2024).
12. H. Lin, E. Van Wagner, B. D. Freeman, L. G. Toy, R. P. Gupta, Plasticization-enhanced hydrogen purification using polymeric membranes. *Science* **311**, 639–642 (2006).
13. Y. Han, W. S. W. Ho, Recent advances in polymeric facilitated transport membranes for carbon dioxide separation and hydrogen purification. *J. Polym. Sci.* **58**, 2435–2449 (2020).
14. L. Zhu, D. Yin, Y. Qin, S. Konda, S. Zhang, A. Zhu, S. Liu, T. Xu, M. T. Swihart, H. Lin, Sorption-enhanced mixed matrix membranes with facilitated hydrogen transport for hydrogen purification and CO_2 capture. *Adv. Funct. Mater.* **29**, 1904357 (2019).

15. L. Hu, K. Chen, W. I. Lee, K. Kisslinger, C. Rumsey, S. Fan, V. T. Bui, N. Esmaeili, T. Tran, Y. Ding, M. Trebbin, C. Y. Nam, M. T. Swihart, H. Lin, Palladium-percolated networks enabled by low loadings of branched nanorods for enhanced H_2 separations. *Adv. Mater.* **35**, e2301007 (2023).
16. L. Hu, W. I. Lee, S. Roy, A. Subramanian, K. Kisslinger, L. Zhu, S. Fan, S. Hwang, V. T. Bui, T. Tran, G. Zhang, Y. Ding, P. M. Ajayan, C. Y. Nam, H. Lin, Hierarchically porous and single Zn atom-embedded carbon molecular sieves for H_2 separations. *Nat. Commun.* **15**, 5688 (2024).
17. H. E. Holmes, S. Banerjee, A. Vallace, R. P. Lively, C. W. Jones, M. J. Realff, Tuning sorbent properties to reduce the cost of direct air capture. *Energ. Environ. Sci.* **17**, 4544–4559 (2024).
18. Z. Zhou, T. Ma, H. Zhang, S. Chheda, H. Li, K. Wang, S. Ehrling, R. Giovine, C. Li, A. H. Alawadhi, M. M. Abduljawad, M. O. Alawad, L. Gagliardi, J. Sauer, O. M. Yaghi, Carbon dioxide capture from open air using covalent organic frameworks. *Nature* **635**, 96–101 (2024).
19. A. Vallace, Y. Ren, C. W. Jones, R. P. Lively, Kinetic model describing self-limiting CO_2 diffusion in supported amine adsorbents. *Chem. Eng. J.* **472**, 144838 (2023).
20. T. Tran, S. Singh, S. Cheng, H. Lin, Scalable and highly porous membrane adsorbents for direct air capture of CO_2. *ACS Appl. Mater. Interfaces* **16**, 22715–22723 (2024).
21. B. Wang, Z. Qiao, J. Xu, J. Wang, X. Liu, S. Zhao, Z. Wang, M. D. Guiver, Unobstructed ultrathin gas transport channels in composite membranes by interfacial self-assembly. *Adv. Mater.* **32**, e1907701 (2020).
22. S. Hu, W.-X. Li, Sabatier principle of metal-support interaction for design of ultrastable metal nanocatalysts. *Science* **374**, 1360–1365 (2021).
23. K. Wilpiszewska, T. Spychaj, Chemical modification of starch with hexamethylene diisocyanate derivatives. *Carbohydr. Polym.* **70**, 334–340 (2007).
24. F. Lou, A. Zhang, G. Zhang, L. Ren, X. Guo, C. Song, Enhanced kinetics for CO_2 sorption in amine-functionalized mesoporous silica nanosphere with inverted cone-shaped pore structure. *Appl. Energy* **264**, 114637 (2020).
25. X. Deng, C. Zou, Y. Han, L.-C. Lin, W. W. Ho, Computational evaluation of carriers in facilitated transport membranes for postcombustion carbon capture. *J. Phys. Chem. C* **124**, 25322–25330 (2020).
26. J. Wu, C. Liang, A. Naderi, T. Chung, Tunable supramolecular cavities molecularly homogenized in polymer membranes for ultraefficient precombustion CO_2 capture. *Adv. Mater.* **34**, 2105156 (2021).
27. L. Hu, V. T. Bui, A. Krishnamurthy, S. Fan, W. Guo, S. Pal, X. Chen, G. Zhang, Y. Ding, R. P. Singh, M. Lupion, H. Lin, Tailoring sub-3.3 Å ultramicropores in advanced carbon molecular sieve membranes for blue hydrogen production. *Sci. Adv.* **8**, eabl8160 (2022).
28. Y.-W. Hong, L. Laysandra, Y.-C. Chiu, D.-Y. Kang, Vacuum-assisted self-healing amphiphilic copolymer membranes for gas separation. *ACS Appl. Mater. Interfaces* **15**, 34075–34086 (2023).
29. J. Liu, W. Duan, J. Song, X. Guo, Z. Wang, X. Shi, J. Liang, J. Wang, P. Cheng, Y. Chen, M. J. Zaworotko, Z. Zhang, Self-healing hyper-cross-linked metal–organic polyhedra (HCMOPs) membranes with antimicrobial activity and highly selective separation properties. *J. Am. Chem. Soc.* **141**, 12064–12070 (2019).
30. W. Guo, T. N. Tran, H. Mondal, S. Schaefer, L. Huang, H. Lin, Superior CO_2/N_2 separation performance of highly branched Poly(1, 3 dioxolane) plasticized by polyethylene glycol. *J. Membr. Sci.* **648**, 120352 (2022).
31. M. Cao, C. Han, S. Wang, J. Yu, X. Zhou, F. Yang, Y. Chen, Investigation of density, viscosity and derived thermodynamic properties of CO_2-free and CO_2-loaded poly(ethylene imine) aqueous systems at different temperatures and 0.1 MPa. *J. Molecul. Liquids* **377**, 121523 (2023).
32. L. Hu, S. Pal, H. Nguyen, V. Bui, H. Lin, Molecularly engineering polymeric membranes for H_2/CO_2 separation at 100–300°C. *J. Polym. Sci.* **58**, 2467–2481 (2020).
33. G. Zhang, V. Bui, Y. Yin, E. H. R. Tsai, C. Y. Nam, H. Lin, Carbon capture membranes based on amorphous polyether nanofilms enabled by thickness confinement and interfacial engineering. *ACS Appl. Mater. Interfaces* **15**, 35543–35551 (2023).
34. P. Giannozzi, O. Andreussi, T. Brumme, O. Bunau, M. Buongiorno Nardelli, M. Calandra, R. Car, C. Cavazzoni, D. Ceresoli, M. Cococcioni, N. Colonna, I. Carnimeo, A. Dal Corso, S. de Gironcoli, P. Delugas, R. A. DiStasio Jr., A. Ferretti, A. Floris, G. Fratesi, G. Fugallo, R. Gebauer, U. Gerstmann, F. Giustino, T. Gorni, J. Jia, M. Kawamura, H. Y. Ko, A. Kokalj, E. Küçükbenli, M. Lazzeri, M. Marsili, N. Marzari, F. Mauri, N. L. Nguyen, H. V. Nguyen, A. Otero-de-la-Roza, L. Paulatto, S. Poncé, D. Rocca, R. Sabatini, B. Santra, M. Schlipf, A. P. Seitsonen, A. Smogunov, I. Timrov, T. Thonhauser, P. Umari, N. Vast, X. Wu, S. Baroni, Advanced capabilities for materials modelling with Quantum ESPRESSO. *J. Phys. Condens. Matter* **29**, 465901 (2017).
35. P. Giannozzi, S. Baroni, N. Bonini, M. Calandra, R. Car, C. Cavazzoni, D. Ceresoli, G. L. Chiarotti, M. Cococcioni, I. Dabo, A. Dal Corso, S. de Gironcoli, S. Fabris, G. Fratesi, R. Gebauer, U. Gerstmann, C. Gougoussis, A. Kokalj, M. Lazzeri, L. Martin-Samos, N. Marzari, F. Mauri, R. Mazzarello, S. Paolini, A. Pasquarello, L. Paulatto, C. Sbraccia, S. Scandolo, G. Sclauzero, A. P. Seitsonen, A. Smogunov, P. Umari, R. M. Wentzcovitch, QUANTUM ESPRESSO: A modular and open-source software project for quantum simulations of materials. *J. Phys. Condens. Matter* **21**, 395502 (2009).
36. J. Klimeš, D. R. Bowler, A. Michaelides, Van der Waals density functionals applied to solids. *Phys. Rev. B* **83**, 195131 (2011).
37. H. Nguyen, M. Wang, M. Y. Hsiao, K. Nagai, Y. Ding, H. Lin, Suppression of crystallization in thin films of cellulose diacetate and its effect on CO_2/CH_4 separation properties. *J. Membr. Sci.* **586**, 7–14 (2019).
38. T. Tran, Y. Fu, D. Jiang, H. Lin, Simulation and experiment of CO_2 philicity and separation in carbonate-rich polymers. *Macromolecules* **55**, 9860–9867 (2022).
39. V. Bondar, B. Freeman, I. Pinnau, Gas sorption and characterization of poly(ether-*b*-amide) segmented block copolymers. *J. Polym. Sci. Part B Polym. Phys.* **37**, 2463–2475 (1999).
40. R. D. Raharjo, H. Lin, D. F. Sanders, B. D. Freeman, S. Kalakkunnath, D. S. Kalika, Relation between network structure and gas transport in crosslinked poly (propylene glycol diacrylate). *J. Membr. Sci.* **283**, 253–265 (2006).
41. L. F. Villalobos, R. Hilke, F. H. Akhtar, K. V. Peinemann, Fabrication of polybenzimidazole/palladium nanoparticles hollow fiber membranes for hydrogen purification. *Adv. Energy Mater.* **8**, 1701567 (2018).
42. T. Yang, G. Shi, T. S. Chung, Symmetric and asymmetric zeolitic imidazolate frameworks (ZIFs)/polybenzimidazole (PBI) nanocomposite membranes for hydrogen purification at high temperatures. *Adv. Energy Mater.* **2**, 1358–1367 (2012).
43. Z. Ali, F. Pacheco, E. Litwiller, Y. Wang, Y. Han, I. Pinnau, Ultra-selective defect-free interfacially polymerized molecular sieve thin-film composite membranes for H_2 purification. *J. Mater. Chem. A* **6**, 30–35 (2018).
44. M. Shan, X. Liu, X. Wang, I. Yarulina, B. Seoane, F. Kapteijn, J. Gascon, Facile manufacture of porous organic framework membranes for precombustion CO_2 capture. *Sci. Adv.* **4**, eaau1698 (2018).
45. M. Shan, X. Liu, X. Wang, Z. Liu, H. Iziyi, S. Ganapathy, J. Gascon, F. Kapteijn, Novel high performance poly(*p*-phenylene benzobisimidazole) (PBDI) membranes fabricated by interfacial polymerization for H_2 separation. *J. Mater. Chem. A* **7**, 8929–8937 (2019).
46. J. Seong, W. H. Lee, J. Lee, S. Y. Lee, Y. S. do, J. Y. Bae, S. J. Moon, C. H. Park, H. J. Jo, J. S. Kim, K. R. Lee, W. S. Hung, J. Y. Lai, Y. Ren, C. J. Roos, R. P. Lively, Y. M. Lee, Microporous polymers with cascaded cavities for controlled transport of small gas molecules. *Sci. Adv.* **7**, eabi9062 (2021).
47. L. Liu, C.-E. Ku, C. Zhang, Petrified hollow fiber membranes with hierarchical pores. *ACS Mater. Lett.* **4**, 938–943 (2022).
48. L. Lei, F. Pan, A. Lindbråthen, X. Zhang, M. Hillestad, Y. Nie, L. Bai, X. He, M. D. Guiver, Carbon hollow fiber membranes for a molecular sieve with precise-cutoff ultramicropores for superior hydrogen separation. *Nat. Commun.* **12**, 268 (2021).
49. K. He, Y. Hu, Z. X. Low, R. Wang, F. Wang, H. Ma, X. Chen, D. R. MacFarlane, H. Wang, Metal oxyhydroxide nanosheet-assisted fabrication of ultrathin carbon molecular sieve membrane for hydrogen separation. *J. Mater. Chem. A* **10**, 18095–18102 (2022).
50. P. T. Ngamou, M. Ivanova, O. Guillon, W. A. Meulenberg, High-performance carbon molecular sieve membranes for hydrogen purification and pervaporation dehydration of organic solvents. *J. Mater. Chem. A* **7**, 7082–7091 (2019).
51. G. S. Foo, J. J. Lee, C. H. Chen, S. E. Hayes, C. Sievers, C. W. Jones, Elucidation of surface species through in situ FTIR spectroscopy of carbon dioxide adsorption on amine-grafted SBA-15. *ChemSusChem* **10**, 266–276 (2017).
52. X. Wang, X. Ma, V. Schwartz, J. C. Clark, S. H. Overbury, S. Zhao, X. Xu, C. Song, A solid molecular basket sorbent for CO_2 capture from gas streams with low CO_2 concentration under ambient conditions. *Phys. Chem. Chem. Phys.* **14**, 1485–1492 (2012).
53. L. Hu, V. T. Bui, S. Fan, W. Guo, S. Pal, Y. Ding, H. Lin, Supramolecular assemblies of polybenzimidazole and aromatic polycarboxylic acids with superior mechanical and H_2/CO_2 separation properties. *J. Mater. Chem. A* **10**, 10872–10879 (2022).
54. L. Zhu, M. T. Swihart, H. Lin, Unprecedented size-sieving ability in polybenzimidazole doped with polyprotic acids for membrane H_2/CO_2 separation. *Energ. Environ. Sci.* **11**, 94–100 (2018).
55. Dassault Systèmes, BIOVIA Materials Studio Amorphous Cell (2024).
56. A. K. Rappé, C. J. Casewit, K. Colwell, W. A. Goddard III, W. M. Skiff, UFF, a full periodic table force field for molecular mechanics and molecular dynamics simulations. *J. Am. Chem. Soc.* **114**, 10024–10035 (1992).
57. L. Martínez, R. Andrade, E. Birgin, J. M. Packmol, PACKMOL: A package for building initial configurations for molecular dynamics simulations. *J. Comput. Chem.* **30**, 2157–2164 (2009).
58. W. Humphrey, A. Dalke, K. Schulten, VMD: Visual molecular dynamics. *J. Mol. Graph.* **14**, 33–38 (1996).
59. J. J. Potoff, J. I. Siepmann, Vapor–liquid equilibria of mixtures containing alkanes, carbon dioxide, and nitrogen. *AIChE J.* **47**, 1676–1682 (2001).
60. Y. Sun, R. F. DeJaco, Z. Li, D. Tang, S. Glante, D. S. Sholl, C. M. Colina, R. Q. Snurr, M. Thommes, M. Hartmann, J. I. Siepmann, Fingerprinting diverse nanoporous materials for optimal hydrogen storage conditions using meta-learning. *Sci. Adv.* **7**, eabg3983 (2021).

61. R. W. Hockney, J. W. Eastwood, *Computer Simulation Using Particles* (CRC Press, 2021).
62. M. P. Allen, D. J. Tildesley, *Computer Simulation of Liquids* (Oxford Univ. Press, 2017).
63. I.-C. Yeh, M. L. Berkowitz, Ewald summation for systems with slab geometry. *J. Chem. Phys.* **111**, 3155–3162 (1999).
64. S. Nosé, A unified formulation of the constant temperature molecular dynamics methods. *J. Chem. Phys.* **81**, 511–519 (1984).
65. W. G. Hoover, Canonical dynamics: Equilibrium phase-space distributions. *Phys. Rev. A* **31**, 1695–1697 (1985).
66. A. P. Thompson, H. M. Aktulga, R. Berger, D. S. Bolintineanu, W. M. Brown, P. S. Crozier, P. J. in 't Veld, A. Kohlmeyer, S. G. Moore, T. D. Nguyen, R. Shan, M. J. Stevens, J. Tranchida, C. Trott, S. J. Plimpton, LAMMPS-A flexible simulation tool for particle-based materials modeling at the atomic, meso, and continuum scales. *Comput. Phys. Commun.* **271**, 108171 (2022).
67. H. Xu, R. Cabriolu, B. Smit, Effects of degrees of freedom on calculating diffusion properties in nanoporous materials. *J. Chem. Theory Comput.* **18**, 2826–2835 (2022).
68. J. Baker, An algorithm for the location of transition states. *J. Comput. Chem.* **7**, 385–395 (1986).
69. D. Dubbeldam, S. Calero, D. E. Ellis, R. Q. Snurr, RASPA: Molecular simulation software for adsorption and diffusion in flexible nanoporous materials. *Mol. Simul.* **42**, 81–101 (2016).
70. A. Jana, D. S. Bergsman, J. C. Grossman, Adsorption-based membranes for air separation using transition metal oxides. *Nanoscale Adv.* **3**, 4502–4512 (2021).
71. J. Liu, C. R. P. Fulong, L. Hu, L. Huang, G. Zhang, T. R. Cook, H. Lin, Interpenetrating networks of mixed matrix materials comprising metal-organic polyhedra for membrane CO_2 capture. *J. Membr. Sci.* **606**, 118122 (2020).
72. L. Huang, W. Guo, H. Mondal, S. Schaefer, T. N. Tran, S. Fan, Y. Ding, H. Lin, Effect of branch length on the structural and separation properties of hyperbranched poly (1, 3-dioxolane). *Macromolecules* **55**, 382–389 (2021).
73. L. Hu, V. T. Bui, L. Huang, R. P. Singh, H. Lin, Facilely cross-linking polybenzimidazole with polycarboxylic acids to improve H_2/CO_2 separation performance. *ACS Appl. Mater. Interfaces* **13**, 12521–12530 (2021).
74. S. Kulkarni, S. Stern, The diffusion of CO_2, CH_4, C_2H_4, and C_3H_8 in polyethylene at elevated pressures. *J. Polym. Sci. Polym. Phys. Ed.* **21**, 441–465 (1983).
75. Y. Zhang, I. H. Musseman, J. P. Ferraris, K. J. Balkus, Gas permeability properties of Matrimid® membranes containing the metal-organic framework Cu-BPY-HFS. *J. Membr. Sci.* **313**, 170–181 (2008).
76. A. C. Puleo, D. R. Paul, S. S. Kelley, The effect of degree of acetylation on gas sorption and transport behavior in cellulose acetate. *J. Membr. Sci.* **47**, 301–332 (1989).
77. C. Aitken, W. Koros, D. Paul, Effect of structural symmetry on gas transport properties of polysulfones. *Macromolecules* **25**, 3424–3434 (1992).
78. W. Koros, G. Fleming, S. Jordan, T. Kim, H. Hoehn, Polymeric membrane materials for solution-diffusion based permeation separations. *Prog. Polym. Sci.* **13**, 339–401 (1988).
79. X. Li, R. P. Singh, K. W. Dudeck, K. A. Berchtold, B. C. Benicewicz, Influence of polybenzimidazole main chain structure on H_2/CO_2 separation at elevated temperatures. *J. Membr. Sci.* **461**, 59–68 (2014).
80. L. Zhu, M. T. Swihart, H. Lin, Tightening polybenzimidazole (PBI) nanostructure via chemical cross-linking for membrane H_2/CO_2 separation. *J. Mater. Chem. A* **5**, 19914–19923 (2017).
81. K. A. Stevens, J. D. Moon, H. Borjigin, R. Liu, R. M. Joseph, J. S. Riffle, B. D. Freeman, Influence of temperature on gas transport properties of tetraaminodiphenylsulfone (TADPS) based polybenzimidazoles. *J. Membr. Sci.* **593**, 117427 (2020).
82. L. Hu, V. T. Bui, S. Pal, W. Guo, A. Subramanian, K. Kisslinger, S. Fan, C. Y. Nam, Y. Ding, H. Lin, In situ growth of crystalline and polymer-incorporated amorphous ZIFs in polybenzimidazole achieving hierarchical nanostructures for carbon capture. *Small* **18**, e2201982 (2022).
83. L. Hu, S. Fan, L. Huang, V. T. Bui, T. Tran, K. Chen, Y. Ding, M. T. Swihart, H. Lin, Supramolecular polymer networks of ion-coordinated polybenzimidazole with simultaneously improved H_2 permeability and H_2/CO_2 selectivity. *Macromolecules* **55**, 6901–6910 (2022).
84. A. Naderi, A. A. Tashvigh, T. Chung, H_2/CO_2 separation enhancement via chemical modification of polybenzimidazole nanostructure. *J. Membr. Sci.* **572**, 343–349 (2019).
85. J. Wu, T. Chung, Supramolecular polymer network membranes with molecular-sieving nanocavities for efficient pre-combustion CO_2 capture. *Small Methods* **6**, 2101288 (2021).
86. M. Huang, K. Lu, Z. Wang, X. Bi, Y. Zhang, J. Jin, Thermally cross-linked amidoxime-functionalized polymers of intrinsic microporosity membranes for highly selective hydrogen separation. *ACS Sustain. Chem. Eng.* **9**, 9426–9435 (2021).
87. F. Li, Y. Xiao, Y. K. Ong, T. S. Chung, UV-rearranged PIM-1 polymeric membranes for advanced hydrogen purification and production. *Adv. Energy Mater.* **2**, 1456–1466 (2012).
88. W. F. Yong, F. Y. Li, T.-S. Chung, Y. W. Tong, Highly permeable chemically modified PIM-1/Matrimid membranes for green hydrogen purification. *J. Mater. Chem. A* **1**, 13914–13925 (2013).
89. K. Min, D. R. Paul, Effect of tacticity on permeation properties of poly (methyl methacrylate). *J. Polym. Sci. Part B Polym. Phys.* **26**, 1021–1033 (1988).
90. G. Illing, K. Hellgardt, M. Schonert, R. J. Wakeman, A. Jungbauer, Towards ultrathin polyaniline films for gas separation. *J. Membr. Sci.* **253**, 199–208 (2005).
91. D. Weinkauf, D. Paul, Gas transport properties of thermotropic liquid-crystalline copolyesters. II. The effects of copolymer composition. *J. Polym. Sci. Part B Polym. Phys.* **30**, 837–849 (1992).
92. S.-J. Ahn, A. Takagaki, T. Sugawara, R. Kikuchi, S. T. Oyama, Permeation properties of silica-zirconia composite membranes supported on porous alumina substrates. *J. Membr. Sci.* **526**, 409–416 (2017).
93. M. Dakhchoune, L. F. Villalobos, R. Semino, L. Liu, M. Rezaei, P. Schouwink, C. E. Avalos, P. Baade, V. Wood, Y. Han, M. Ceriotti, K. V. Agrawal, Gas-sieving zeolitic membranes fabricated by condensation of precursor nanosheets. *Nat. Mater.* **20**, 362–369 (2021).
94. Y. Peng, Y. Li, Y. Ban, W. Yang, Two-dimensional metal-organic framework nanosheets for membrane-based gas separation. *Angew. Chem. Int. Ed. Engl.* **56**, 9757–9761 (2017).
95. P. Zhang, Q. Wang, Y. Zhang, M. Lin, X. Zhou, A. David, A. Ustyuzhanin, M. Chen, M. I. Katsnelson, M. Trubyanov, K. S. Novoselov, D. V. Andreeva, Strain-induced crumpling of graphene oxide lamellas to achieve fast and selective transport of H_2 and CO_2. *Nat. Nanotechnol.* **20**, 1254–1261 (2025).
96. Y. Ying, M. Tong, S. Ning, S. K. Ravi, S. B. Peh, S. C. Tan, S. J. Pennycook, D. Zhao, Ultrathin two-dimensional membranes assembled by ionic covalent organic nanosheets with reduced apertures for gas separation. *J. Am. Chem. Soc.* **142**, 4472–4480 (2020).
97. J. Shen, G. Liu, Y. Ji, Q. Liu, L. Cheng, K. Guan, M. Zhang, G. Liu, J. Xiong, J. Yang, W. Jin, 2D MXene nanofilms with tunable gas transport channels. *Adv. Funct. Mater.* **28**, 1801511 (2018).
98. A. Achari, S. Sahana, M. Eswaramoorthy, High performance MoS_2 membranes: Effects of thermally driven phase transition on CO_2 separation efficiency. *Energ. Environ. Sci.* **9**, 1224–1228 (2016).
99. L. F. Villalobos, M. T. Vahdat, M. Dakhchoune, Z. Nadizadeh, M. Mensi, E. Oveisi, D. Campi, N. Marzari, K. V. Agrawal, Large-scale synthesis of crystalline g-C_3N_4 nanosheets and high-temperature H_2 sieving from assembled films. *Sci. Adv.* **6**, eaay9851 (2020).
100. H. Song, Y. Wei, H. Qi, Tailoring pore structures to improve the permselectivity of organosilica membranes by tuning calcination parameters. *J. Mater. Chem. A* **5**, 24657–24666 (2017).
101. J. Fu, S. das, G. Xing, T. Ben, V. Valtchev, S. Qiu, Fabrication of COF-MOF composite membranes and their highly selective separation of H_2/CO_2. *J. Am. Chem. Soc.* **138**, 7673–7680 (2016).
102. S. Huang, M. Dakhchoune, W. Luo, E. Oveisi, G. He, M. Rezaei, J. Zhao, D. T. L. Alexander, A. Züttel, M. S. Strano, K. V. Agrawal, Single-layer graphene membranes by crack-free transfer for gas mixture separation. *Nat. Commun.* **9**, 2632 (2018).
103. H. Guo, G. Kong, G. Yang, J. Pang, Z. Kang, S. Feng, L. Zhao, L. Fan, L. Zhu, A. Vicente, P. Peng, Z. Yan, D. Sun, S. Mintova, Cross-linking between sodalite nanoparticles and graphene oxide in composite membranes to trigger high gas permeance, selectivity, and stability in hydrogen separation. *Angew. Chem. Int. Ed. Engl.* **59**, 6284–6288 (2020).
104. H. Fan, M. Peng, I. Strauss, A. Mundstock, H. Meng, J. Caro, MOF-in-COF molecular sieving membrane for selective hydrogen separation. *Nat. Commun.* **12**, 38 (2021).
105. C. Covarrubias, R. Quijada, Preparation of aluminophosphate/polyethylene nanocomposite membranes and their gas permeation properties. *J. Membr. Sci.* **358**, 33–42 (2010).
106. G. Dlubek, K. Saarinen, H. Fretwell, The temperature dependence of the local free volume in polyethylene and polytetrafluoroethylene: A positron lifetime study. *J. Polym. Sci. Part B Polym. Phys.* **36**, 1513–1528 (1998).
107. J. Liu, S. Zhang, D. E. Jiang, C. M. Doherty, A. J. Hill, C. Cheng, H. B. Park, H. Lin, Highly polar but amorphous polymers with robust membrane CO_2/N_2 separation performance. *Joule* **3**, 1881–1894 (2019).
108. A. Alentiev, E. Drioli, M. Gokzhaev, G. Golemme, O. Ilinich, A. Lapkin, V. Volkov, Y. Yampolskii, Gas permeation properties of phenylene oxide polymers. *J. Membr. Sci.* **138**, 99–107 (1998).
109. C. Zhang, R. P. Lively, K. Zhang, J. R. Johnson, O. Karvan, W. J. Koros, Unexpected molecular sieving properties of zeolitic imidazolate framework-8. *J. Phys. Chem. Lett.* **3**, 2130–2134 (2012).
110. S. S. Hosseini, T. S. Chung, Carbon membranes from blends of PBI and polyimides for N_2/CH_4 and CO_2/CH_4 separation and hydrogen purification. *J. Membr. Sci.* **328**, 174–185 (2009).
111. R. P. Singh, G. J. Dahe, K. W. Dudeck, C. F. Welch, K. A. Berchtold, High temperature polybenzimidazole hollow fiber membranes for hydrogen separation and carbon dioxide capture from synthesis gas. *Energy Procedia* **63**, 153–159 (2014).
112. T. C. Merkel, "Novel polymer membrane process for pre-combustion CO_2 capture from coal-fired syngas, Final report to the US DOE, FE0001124," (Membrane Technology and Research, Inc., 2011).
113. I. Jayaweera, P. Jayaweera, S. Bhamidi, R. Elmore, E. Perea, X. Wang, "Development of a pre-combustion CO_2 capture process using high-temperature PBI hollow-fiber membranes," in *14th Greenhouse Gas Control Technologies Conference Melbourne* (Social Science Research Network, 2018), pp. 21–26.

Acknowledgments: This research used computational resources provided by the Center for Computational Research at the University at Buffalo. **Funding:** This work was supported by the US Department of Energy (DOE) awards DE-FE0031636 and DE-FE0032209. L.H. thanks the startup Funding for the "Hundred-Talent" Program of Zhejiang University (115000*1942225R3).
Author contributions: Conceptualization: L.H., G.Z., H.L., and A.J.G. Methodology: L.H., K.S., P.Z., G.Z., K.F., and A.J.G. Investigation: L.H., H.L., K.S., P.Z., G.Z., T.T., A.J.G., and N.E. Visualization: L.H., K.S., P.Z., and A.J.G. Resources: L.H., H.L., G.Z., P.Z., and A.J.G. Data curation: L.H., G.Z., K.S., and A.J.G. Validation: L.H., G.Z., K.S., P.Z., A.J.G., and N.E. Formal analysis: K.S., P.Z., and A.J.G. Software: L.H., K.S., and A.J.G. Funding acquisition: H.L. Supervision: H.L. and Y.D. Project administration: L.H., H.L., G.Z., and A.J.G. Writing—original draft: L.H., A.J.G. Writing—review and editing: H.L., L.H., K.S., Y.D., P.Z., G.Z., T.T., and A.J.G. **Competing interests:** The authors declare that they have no competing interests. **Data and materials availability:** All data needed to evaluate the conclusions in the paper are present in the paper and/or the Supplementary Materials.

Submitted 25 May 2025
Accepted 24 October 2025
Published 21 November 2025
10.1126/sciadv.adz2830